Auxiliary Vehicle Positioning Based on Robust DOA Estimation With Unknown Mutual Coupling

Fangqing Wen, *Member, IEEE*, Juan Wang, Junpeng Shi, and Guan Gui, *Senior Member, IEEE*

***Abstract*—As an important branch of the Internet of Vehicles (IoV), vehicle positioning has drawn extensive attention. Traditional positioning systems based on a global positioning system incur long delays, and may fail due to obstructions. In this article, we propose an auxiliary positioning architecture, whose core is to estimate the direction of arrival (DOA) of signals from landmarks, such as wireless access points, utilizing a sensor array in the vehicle. Due to space limitations, the array may be placed in an arbitrary geometry and may suffer from unknown mutual coupling. Most algorithms are only effective for sensor arrays with special geometries, e.g., a uniform linear array or rectangular array. To tackle this problem, an improved multiple signal classification algorithm is derived, which is superior to the state-of-the-art iterative method from the perspective of computational complexity. Detailed analysis concerning identifiability, computational complexity, and Cramér–Rao bounds are given. The simulation results verify the improvement of the proposed DOA estimation algorithm. The proposed architecture can obtain robust self-localization with existing vehicular *ad hoc* networks, and it can collaborate with other positioning systems to provide a safe driving environment.**

***Index Terms*—Arbitrary geometry, direction-of-arrival (DOA) estimation, Internet of Vehicles (IoV), mutual coupling, sensor array, vehicle positioning.**

I. Introduction

RECENT decades have witnessed explosive growth in the demands on the Internet of Vehicles (IoV) [1]–[8]. Generally speaking, the IoV refers to the infrastructure that connects vehicles to intervehicle networks [9]–[12], intravehicle networks, and the vehicular mobile Internet. The IoV is a complex system that integrates vehicle technology with detection [13], networks [14], cloud computing [15]–[17], and control. It aims to offer safe and comfortable driving services and may profoundly change human lives. Vehicle location awareness is vital for emerging IoV [18], and it enables numerous applications, such as navigation, collision warning, and emergency rescue [19]. It is well known that vehicle location can be obtained via commercial global positioning systems (GPSs). However, the reliability of GPS systems is too poor (long latency and inadequate accuracy) to provide a safe driving environment. Moreover, GPS systems may fail to work due to imperfect environments, such as tunnels and cloud cover.

Advanced sensors (e.g., radar, lidar, and camera) have been widely investigated to overcome the above disadvantages. Among various positioning techniques, cooperative positioning systems are common for reasons of cost, latency, and reliability [20]. Cooperative positioning techniques use wireless communication devices, such as wireless access points (APs) and cellular devices, to estimate the vehicle position [21]. A vehicles position can be achieved based on the four principles of radio signal strength (RSS), time of arrival (TOA), time difference of arrival (TDOA), and direction of arrival (DOA). In [22] and [23], RSS approaches are adopted to achieve target vehicle localization, where the spatial fading properties of signals must be known as a prior. Due to the complexity of wireless channels, the fading characteristics are difficult to obtain accurately, hence the RSS approach has limited accuracy. The TOA and TDOA algorithms were proposed in [24], [25], and [26], respectively. The perfect synchronization of clocks between all nodes is essential to both approaches, and this is difficult to achieve in practice. Their performance is highly sensitive to time-difference measurements, making it difficult to obtain high-accuracy vehicle positions. Hence, the DOA approaches become good choices. Their positioning performance depends only on the accuracy of DOA estimation, which can be easily measured via a radio array. DOA approaches were proposed in [27] and [28], in which the DOA of the incoming signal is measured using at least three nodes. Wymeersch *et al.* [29] and Abu-Shaban *et al.* [30] discussed positioning approaches that combine angle and delay, which are less costly than DOA approaches, since they require fewer nodes. However, like their TOA and TDOA counterparts, the positioning accuracy of the combination approaches is sensitive to delay measurement. To avoid measuring delay information, we focus on a DOA-aware vehicle positioning system.

DOA estimation has a rich history, stretching over 60 years. Many excellent estimators have been proposed [31]–[36],

Manuscript received January 14, 2020; revised February 17, 2020; accepted March 4, 2020. Date of publication March 10, 2020; date of current version June 12, 2020. This work was supported in part by the National Natural Science Foundation of China under Grant 61601504, Grant 61701046, and Grant 61701258; in part by the National Science and Technology Major Project of the Ministry of Science and Technology of China under Grant TC190A3WZ-2; in part by the Jiangsu Specially Appointed Professor under Grant RK002STP16001; in part by the Innovation and Entrepreneurship of Jiangsu High-Level Talent under Grant CZ0010617002; in part by the Six Top Talents Program of Jiangsu under Grant XYDXX-010; and in part by the 1311 Talent Plan of Nanjing University of Posts and Telecommunications. *(Corresponding author: Junpeng Shi.)*

Fangqing Wen is with the School of Electronics and Information, Yangtze University, Jingzhou 434023, China, and also with the State Key Laboratory of Marine Resource Utilization in South China Sea, Hainan University, Haikou 570228, China.

Juan Wang and Guan Gui are with the College of Telecommunications and Information Engineering, Nanjing University of Posts and Telecommunications, Nanjing 210003, China.

Junpeng Shi is with the National University of Defense Technology, Hefei 230037, China (e-mail: 15667081720@163.com).

Digital Object Identifier 10.1109/JIOT.2020.2979771

such as estimation method of signal parameters via rotational invariance technique (ESPRIT), multiple signal classification (MUSIC), and tensor estimators. Most estimators rely on a well-calibrated sensor array. In practice, however, sensor array errors are always present and unknown. Typical sensor errors include gain-phase error, position error, and mutual coupling, the last being particularly important. Mutual coupling is caused by the radiation effects of the antenna elements. This will cause a model mismatch in DOA estimation and may lead to seriously degraded estimation performance. Optimal DOA estimation requires a sensor array capable of self-calibration, using its collected signals to simultaneously calibrate the sensor error and perform the desired function. Several efforts have addressed this issue. In [37], an active calibration method was proposed in that required additional instrumental sensors. In [38], an iterative strategy was proposed for performing the joint estimation of DOA and mutual coupling coefficients, which required no auxiliary sources or instrumental sensors. However, such an iterative procedure is computationally inefficient. The recursive rank reduction method was proposed to lessen the computational load in [39]. In [40], DOA estimation and mutual coupling calibration problems were investigated from the Bayesian learning perspective. More recently, an improved Bayesian learning algorithm was derived in [41], and it is capable of solving the off-grid problem. Considering the low-rank properties, sparsity-awarded frameworks have been proposed [42], [43] offering new insights into the mutual coupling problem. Efforts have also been made to improve estimation performance using the extra information of the source signals [44], [45], and the direction-dependent mutual coupling problem has been investigated [46], [47]. The algorithms in [38]–[47] are only suitable for a uniform linear array (ULA). Similar works have been done for uniform circular arrays [48]–[50], uniform rectangular arrays [51], [52], and cross arrays [53].

The aforementioned algorithms are only effective for arrays with special geometries. In such cases, the mutual coupling matrix is assigned a special structure, e.g., symmetric Toeplitz, symmetric circulant, or symmetric block Toeplitz. However, sensors in IoV systems may be irregularly distributed due to space limitations, in which case mutual coupling matrices have few special structures beyond being symmetric, and current algorithms would fail to work. To our knowledge, only [54] has stressed the DOA estimation problem for such scenarios. To relax the mutual coupling requirement in DOA estimation, a two-step alternative method was proposed in [54]. In the first step, the mutual coupling coefficients are interpreted as known priors, and DOA estimation is accomplished via the traditional MUSIC algorithm. In the second step, mutual coupling coefficients are estimated by solving a semi-definite programming problem, using the previously obtained DOAs. Iteration continues until convergence conditions are satisfied. Although the iterative method in [54] is suitable for an arbitrary geometry, it is time consuming, which makes implementation difficult for real-time systems.

In this article, an auxiliary vehicle positioning framework based on robust DOA estimation is proposed that is easily implemented via existing vehicular *ad hoc* networks (VANETs). Moreover, we consider a more realistic scenario in which the sensor array is distributed in an arbitrary geometry, but it suffers from the unknown mutual coupling. A fast DOA estimation algorithm is derived and analyzed. The contributions of this article are as follows.

1) An auxiliary vehicle positioning architecture relying on VANETs and robust DOA estimation is presented. In the proposed framework, low-latency wireless APs, e.g., 5G base stations, are interpreted as landmarks. Vehicles are equipped with an antenna array (for wireless communications), and DOAs from different landmarks are measured to calculate vehicle positions. In addition, the measured results can be uploaded to a cloud platform to collaborate with other positioning systems to provide a safe driving environment. Since wireless APs and antenna arrays are the basic infrastructures of VANETs, the proposed architecture is easily implemented. Unlike the DOA approach in [28], the proposed architecture can achieve onboard positioning without additional hardware.
2) We consider a more practical scenario for DOA estimation. The sensor array is placed in an arbitrary geometry in the vehicle, since sensors suffer from the unknown mutual coupling. The data model for DOA estimation in such a scenario is established, in which mutual coupling between sensors is formulated into a mutual coupling matrix.
3) A fast DOA estimation and mutual coupling self-calibration algorithm is proposed. To pursue robust vehicle positioning, the DOA estimation problem is first linked to the perturbed MUSIC search issue, in which each response vector is corrupted by an unknown mutual coupling matrix. The transformation method in [54] is adopted, hence, the unknown mutual coupling coefficients are extracted into a single vector. Using the rank-reduction property of the transformed matrix, DOA estimation is obtained via one-peak searching, and mutual coefficients are subsequently achieved.
4) We analyze the proposed algorithm in terms of identifiability and computational complexity. Moreover, the Cramér–Rao bound (CRB) with respect to DOA estimation and mutual coupling coefficient estimation is derived. Numerical experiments are designed to show the effectiveness and improvement of the proposed algorithm.

The rest of this article is organized as follows. In Section II, the mathematical model of DOA estimation for an arbitrary sensor array with mutual coupling is formulated. The proposed algorithm is described in Section III, and is theoretically analyzed in Section IV. The simulation results are presented in Section V. Conclusions are discussed in Section VI.

Notations: Throughout this article, lowercase italic letters, e.g., a, boldface lowercase letters, e.g., $\mathbf{a}$, and boldface capital letters, e.g., $\mathbf{A}$, are reserved for scalars, vectors, and matrices, respectively. Other notations are as follows.

1) $\mathbf{A}^{\mathrm{T}}$*:* Transpose of $\mathbf{A}$.
2) $\mathbf{A}^{\mathrm{H}}$*:* Hermitian transpose of $\mathbf{A}$.
3) $\mathbf{A}^{*}$*:* Conjugate of $\mathbf{A}$.

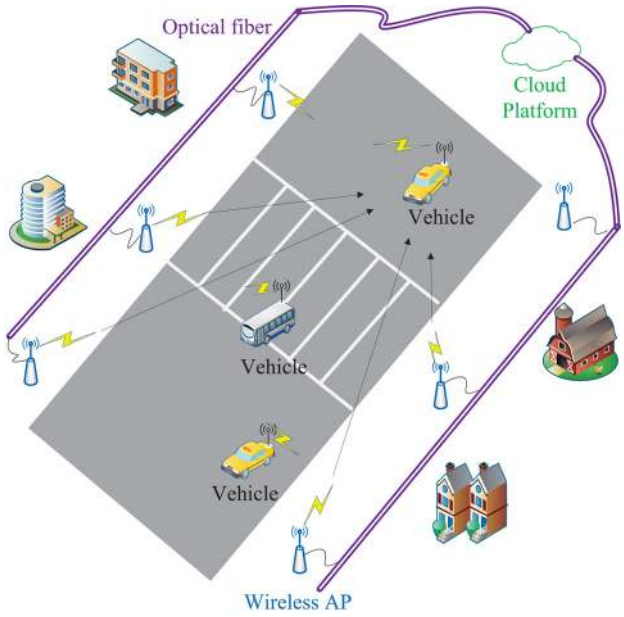

Fig. 1. Illustration of passive vehicle localization system.

4) $\mathbf{A}^{-1}$*:* Inverse of $\mathbf{A}$.
5) $\mathbf{A}^{\dagger}$*:* Pseudoinverse of $\mathbf{A}$.
6) $\mathbf{I}_N$*:* $N \times N$ identity matrix $\mathbf{A}$.
7) $\mathbf{0}$*:* Zero vector.
8) $\mathbf{A}(:, m)$*:* mth column of $\mathbf{A}$.
9) $\mathbf{A}(m, n)$*:* (m, n)th element of $\mathbf{A}$.
10) rank$\{\mathbf{A}\}$*:* Rank of $\mathbf{A}$.
11) det$\{\mathbf{A}\}$*:* Determinant of $\mathbf{A}$.
12) diag$\{a_1, a_2, \ldots, a_N\}$*:* Diagonal matrix whose nth diagonal entity is a_n.
13) $|\mathbf{A}|$*:* Absolute value of $\mathbf{A}$.
14) Re$(\mathbf{A})$*:* Real part of $\mathbf{A}$.
15) Im$(\mathbf{A})$*:* Imaginary part of $\mathbf{A}$.

II. Auxiliary Positioning System and Problem Formulation

A. Auxiliary Positioning System

The architecture of the proposed auxiliary positioning system, depicted in Fig. 1, mainly consists of three modules: 1) vehicle terminal; 2) wireless AP; and 3) cloud platform. The cloud platform provides computing services. The wireless AP is fixed at the roadside. It connects with the cloud platform using optical fiber, and can broadcast location information at a fixed frequency, such as 2.4 or 5 GHz. The vehicle terminal is equipped with an antenna array, and it can receive the signals from the wireless AP. The DOAs are calculated onboard, and the results are uploaded to the cloud platform to realize high-accuracy DOA estimation, which is utilized assist in vehicle localization. In addition, we assume that all the nodes in a local area are well synchronized with the same clock. To synchronize the nodes is a key issue in IOV. Actually, it is hard to synchronize the nodes, even within a local area. Imperfect synchronization will result in an inaccurate time measure. However, it has little impact on DOA approaches. How to synchronize the network is a topic of interest, but it is beyond the scope of this article.

To simplify the analysis, we consider a vehicle equipped with an M-element antenna (sensor) array. The sensors are distributed in the 3-D space [54], and coordinates of the mth $(m = 1, 2, \ldots, M)$ sensor are set to $\mathbf{p}_m = [x_m, y_m, z_m]^{\mathrm{T}}$. It is assumed that K uncorrelated narrowband source signals appear in the far field. The DOA pair (or DOA) of the kth $(k = 1, 2, \ldots, K)$ source is denoted as $\Theta_k = [\theta_k, \phi_k]^{\mathrm{T}}$, where θ_k and ϕ_k are, respectively, the kth elevation angle and the kth azimuth angle. The received array signal can be expressed as [54]

$$\begin{aligned}\mathbf{x}(t) &= \sum_{k=1}^{K} \mathbf{a}(\Theta_k) s_k(t) + \mathbf{n}(t) \\ &= \mathbf{A}\mathbf{s}(t) + \mathbf{n}(t)\end{aligned} \tag{1}$$

where $\mathbf{a}(\Theta_k) \triangleq [\exp\{-j2\pi\tau_{1,k}/\lambda\}, \exp\{-j2\pi\tau_{2,k}/\lambda\}, \ldots, \exp\{-j2\pi\tau_{M,k}/\lambda\}]^{\mathrm{T}} \in \mathbb{C}^{M\times 1}$ is the response vector corresponding to the kth target and λ is the carrier wavelength. $\mathbf{s}_k(t)$ is the kth baseband signal, and $\mathbf{n}(t)$ is the array noise. $\mathbf{A} \triangleq [\mathbf{a}(\Theta_1), \mathbf{a}(\Theta_2), \ldots, \mathbf{a}(\Theta_K)] \in \mathbb{C}^{M\times K}$ is the direction matrix and $\mathbf{s}(t) = [s_1(t), s_2(t), \ldots, s_K(t)]^{\mathrm{T}}$ is the source signal matrix. $\tau_{m,k}$ takes the form

$$\tau_{m,k} = \mathbf{p}_m^{\mathrm{T}} \mathbf{r}_k \tag{2}$$

where $\mathbf{r}_k \triangleq [\cos(\phi_k)\sin(\theta_k), \sin(\phi_k)\sin(\theta_k), \cos(\theta_k)]^{\mathrm{T}}$.

In the presence of mutual coupling, the signal model (1) will be invalid. The mutual coupling effect between an M-element sensor array can be described by an $M \times M$ mutual coupling matrix, which is given by

$$\mathbf{C} = \begin{bmatrix} c_1 & c_2 & c_3 & \cdots & c_M \\ c_2 & c_1 & c_{M-3} & \cdots & c_{M-1} \\ c_3 & c_{M-3} & c_1 & \cdots & c_{M-2} \\ \vdots & \ddots & \vdots & \ddots & \vdots \\ c_M & c_{M-1} & c_{M-2} & \cdots & c_1 \end{bmatrix} \tag{3}$$

where c_m in (p, q) of $\mathbf{C}$ is the mutual coupling coefficient between the pth sensor and qth sensors. Generally, the magnitude of c_m is inversely proportional to the distance between the sensors. As a result, $\mathbf{C}$ is a symmetric matrix and $|c_m| < c_1 = 1$ for any $m > 1$. Obviously, there are at most $1 + [(M(M-1))/2]$ distinct entities in $\mathbf{C}$. Actually, the mutual coupling coefficient is approximated by zero if the distance is larger than a given threshold. Due to the identifiability (see Section IV), we assume that there are at most $Q = M - K$ distinct entities in $\mathbf{C}$. Accordingly, the signal model in (1) with mutual coupling is modified to

$$\mathbf{x}(t) = \mathbf{C}\mathbf{A}\mathbf{s}(t) + \mathbf{n}(t). \tag{4}$$

If the noise $\mathbf{n}(t)$ is Gaussian white, and it is uncorrelated with the source signal $\mathbf{s}(t)$, then the covariance matrix of $\mathbf{x}(t)$ is

$$\mathbf{R} = \mathbf{C}\mathbf{A}\mathbf{R}_s\mathbf{A}^{\mathrm{H}}\mathbf{C}^{\mathrm{H}} + \sigma^2\mathbf{I}_M \tag{5}$$

where $\mathbf{R}_s = \mathrm{diag}\{\delta_1, \delta_2, \ldots, \delta_K\}$ is the covariance matrix of the source signals, δ_k is the power of the kth source, and σ is the noise variance. When L snapshots are available, i.e., $t = 1, 2, \ldots, L$, $\mathbf{R}$ can be estimated as

$$\hat{\mathbf{R}} = \frac{1}{L}\sum_{t=1}^{L}\mathbf{x}(t)\mathbf{x}^{\mathrm{H}}(t). \tag{6}$$

Our ultimate goal is to jointly estimate the DOA and mutual coefficients from $\hat{\mathbf{R}}$.

III. Proposed Positioning Algorithm

A. DOA Estimation With Unknown Mutual Coupling

Performing eigendecomposition on $\hat{\mathbf{R}}$, one can obtain

$$\begin{aligned}\hat{\mathbf{R}} &= \sum_{m=1}^{M}\alpha_m\mathbf{u}_m\mathbf{u}_m^{\mathrm{H}} \\ &= \mathbf{U}_s\Sigma_s\mathbf{U}_s^{\mathrm{H}} + \mathbf{U}_n\Sigma_n\mathbf{U}_n^{\mathrm{H}}\end{aligned} \tag{7}$$

where $\alpha_1 \geq \alpha_2 \geq \cdots \geq \alpha_K > \alpha_{K+1} \geq \cdots \geq \alpha_M$ are the eigenvalues and $\mathbf{u}_m \in \mathbb{C}^{M\times 1}$ is the corresponding eigenvector. Moreover

$$\mathbf{U}_s = [\mathbf{u}_1, \mathbf{u}_2, \ldots, \mathbf{u}_K] \tag{8a}$$

$$\Sigma_s = \mathrm{diag}\{\alpha_1, \alpha_2, \ldots, \alpha_K\} \tag{8b}$$

$$\mathbf{U}_n = \left[\mathbf{u}_{K+1}, \mathbf{u}_{K+2}, \ldots, \mathbf{u}_M\right] \tag{8c}$$

$$\Sigma_n = \mathrm{diag}\{\alpha_{K+1}, \alpha_{K+2}, \ldots, \alpha_M\} \tag{8d}$$

where $\mathbf{U}_s$ and $\mathbf{U}_n$ are usually called the signal subspace and noise subspace, respectively. It is well known that $\mathbf{U}_s$ is orthogonal to $\mathbf{U}_n$, and $\mathbf{U}_s$ spans the same subspace as $\mathbf{C}\mathbf{A}$, hence

$$\mathbf{U}_n^{\mathrm{H}}\mathbf{C}\mathbf{a}(\Theta_k) = \mathbf{0}. \tag{9}$$

Consequently, the MUSIC idea can be adopted for DOA estimation, which tries to optimize

$$\min \quad \mathbf{a}^{\mathrm{H}}(\Theta)\mathbf{C}^{\mathrm{H}}\mathbf{U}_n\mathbf{U}_n^{\mathrm{H}}\mathbf{C}\mathbf{a}(\Theta_k). \tag{10}$$

Usually, a grid consisting of all of the possible DOAs is constructed. By finding the peaks of (10), we can obtain the estimates of DOAs. Unfortunately, the traditional MUSIC algorithm fails to work since $\mathbf{C}$ is unknown. To eliminate the mutual coupling effect, the following result will be utilized.

Theorem [54]: For a matrix $\mathbf{C} \in \mathbb{C}^{M\times M}$ and a vector $\mathbf{a} \in \mathbb{C}^{M\times 1}$, if there are only Q ($Q < M$) distinct entities $\mathbf{c} = [c_1, c_2, \ldots, c_Q]^{\mathrm{T}}$ in $\mathbf{C}$, then the following transformation holds:

$$\mathbf{C}\mathbf{a} = \mathbf{T}\mathbf{c} \tag{11}$$

where $\mathbf{T} \in \mathbb{C}^{M\times Q}$, with the qth ($q = 1, 2, \ldots, Q$) column given by

$$\mathbf{T}(:, q) = \mathbf{J}_q\mathbf{a} \tag{12}$$

and $\mathbf{J}_q$ is defined as

$$\mathbf{J}_q(m, n) = \begin{cases} 1, & \text{if } \mathbf{C}(m, n) = c_q \\ 0, & \text{otherwise.} \end{cases} \tag{13}$$

According to the theorem, we have

$$\mathbf{C}\mathbf{a}(\Theta) = \mathbf{T}(\Theta)\mathbf{c} \tag{14}$$

where $\mathbf{T}(\Theta) \in \mathbb{C}^{M\times Q}$ and $\mathbf{c} \in \mathbb{C}^{Q\times 1}$ are constructed accordingly. Equation (10) can then be rewritten as

$$\min \quad \mathbf{c}^{\mathrm{H}}\underbrace{\mathbf{T}^{\mathrm{H}}(\Theta)\mathbf{U}_n\mathbf{U}_n^{\mathrm{H}}\mathbf{T}(\Theta)}_{\triangleq\mathbf{Q}(\Theta)}\mathbf{c}. \tag{15}$$

Equation (15) is obviously a quadratic optimization problem. To avoid the trivial solution $\mathbf{c} = \mathbf{0}$, we enforce the constraint

$$\mathbf{d}^{\mathrm{H}}\mathbf{c} = \rho \tag{16}$$

where ρ is a constant, and $\mathbf{d} = [1, 0, \ldots, 0]^{\mathrm{T}}$. As a result, (15) is transformed to

$$\min \quad \mathbf{c}^{\mathrm{H}}\mathbf{Q}(\Theta)\mathbf{c} \quad \text{s.t.,} \quad \mathbf{d}^{\mathrm{H}}\mathbf{c}/\rho = 1. \tag{17}$$

The above problem can be solved using the Lagrange multiplier technique. First, we construct a Lagrange function

$$\mathcal{L}(\Theta) = \mathbf{c}^{\mathrm{H}}\mathbf{Q}(\Theta)\mathbf{c} - \tau\left(\mathbf{d}^{\mathrm{H}}\mathbf{c}/\rho - 1\right) \tag{18}$$

where τ is a Lagrange multiplier. Then, letting $\partial\mathcal{L}(\Theta)/\mathbf{c}$ go to zero yields

$$2\mathbf{Q}(\Theta)\mathbf{c} + \frac{\tau}{\rho}\mathbf{d} = \mathbf{0} \tag{19}$$

from which we obtain

$$\mathbf{c} = \xi\mathbf{Q}^{-1}(\Theta)\mathbf{d}/\rho \tag{20}$$

where ξ is a constant. Combined with (16), we have

$$\xi = \frac{\rho^2}{\mathbf{d}^{\mathrm{H}}\mathbf{Q}^{-1}(\Theta)\mathbf{d}}. \tag{21}$$

Inserting (21) into (20) gives

$$\mathbf{c} = \frac{\rho^2\mathbf{Q}^{-1}(\Theta)\mathbf{d}}{\mathbf{d}^{\mathrm{H}}\mathbf{Q}^{-1}(\Theta)\mathbf{d}}. \tag{22}$$

Finally, we can rewrite (17) as

$$\min \quad \frac{|\rho^4|}{\mathbf{d}^{\mathrm{H}}\mathbf{Q}^{-1}(\Theta)\mathbf{d}}. \tag{23}$$

As ρ is a constant, (23) is equal to

$$\max \quad \mathbf{d}^{\mathrm{H}}\mathbf{Q}^{-1}(\Theta)\mathbf{d}. \tag{24}$$

The DOA pair (or DOA) can be estimated by searching the K peaks of (24), after which the mutual coupling coefficients can be estimated by

$$\hat{\mathbf{c}} = \frac{1}{K}\sum_{k=1}^{K}\frac{\rho^2\mathbf{Q}^{-1}\left(\hat{\Theta}_k\right)\mathbf{d}}{\mathbf{d}^{\mathrm{H}}\mathbf{Q}^{-1}\left(\hat{\Theta}_k\right)\mathbf{d}}. \tag{25}$$

Note that $c_1 = 1$, and the scalar effect in (25) can be eliminated by normalization.

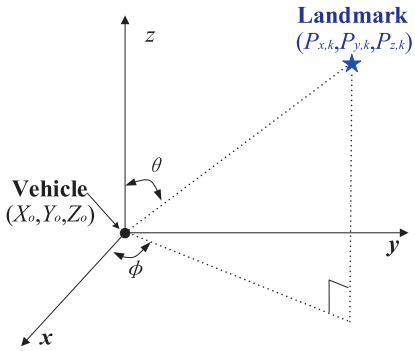

Fig. 2. Diagram for vehicle positioning using 2D-DOA.

It should be pointed out that in the absence of noise, we have

$$\mathbf{c}^{\mathrm{H}}\mathbf{Q}(\Theta)\mathbf{c} = 0 \tag{26}$$

and, as $\mathbf{c} \neq \mathbf{0}$, the necessary condition for (26) is that there is a rank reduction on $\mathbf{Q}(\Theta)$, i.e.,

$$\det\{\mathbf{Q}(\Theta)\} = 0. \tag{27}$$

According to (27), an alternative to DOA estimation is

$$\max \quad \frac{1}{\det\{\mathbf{Q}(\Theta)\}}. \tag{28}$$

B. Vehicle Positioning Using DOA

Once the DOA of a landmark has been obtained, the vehicle position is easily recovered. The positioning principle is depicted in Fig. 2, where the reference sensor with position (X_o,Y_o,Z_o) in the vehicle is set as the coordinate origin. As the position of the kth landmark is known to be $(P_{x,k},P_{y,k},P_{z,k})$, the following equations are established:

$$\tan\theta_k = \frac{P_{y,k} - Y_o}{P_{z,k} - Z_o} \tag{29a}$$

$$\tan\phi_k = \frac{P_{y,k} - Y_o}{P_{x,k} - X_o}. \tag{29b}$$

Since there are three unknown parameters X_o, Y_o, and Z_o, but only two equations, the vehicle position cannot be realized if there is only one landmark. When two landmarks with positions $(P_{x,1},P_{y,1},P_{z,1})$ and $(P_{x,2},P_{y,2},P_{z,2})$ are available, the coordinates of (X_o,Y_o,Z_o) can be determined by

$$X_o = \frac{P_{y,1} - P_{y,2} + \tan\phi_2 P_{z,2} - \tan\phi_1 P_{z,1}}{\tan\phi_2 - \tan\phi_1} \tag{30a}$$

$$Y_o = \frac{\tan\theta_1\tan\theta_2\big(P_{z,1} - P_{z,2}\big) + \tan\theta_1 P_{y,2} - \tan\theta_2 P_{y,1}}{\tan\theta_1 - \tan\theta_2} \tag{30b}$$

$$Z_o = \frac{P_{y,1} - P_{y,2} + \tan\theta_2 P_{z,2} - \tan\theta_1 P_{z,1}}{\tan\theta_2 - \tan\theta_1}. \tag{30c}$$

If more than two landmarks are available, then the estimated accuracy of the coordinates can be improved by averaging various results.

It should be pointed out that the 3-D coordinates of the vehicle rely on 2D-DOA estimation. If we can only obtain 1D-DOA (e.g., the manifold of the sensor array is linear), then we can only determine the 2-D coordinates of the vehicle, as discussed in [28].

To better understand the proposed positioning algorithm, the steps of the algorithm are listed in Table I.

TABLE I
ALGORITHMIC STEPS OF PROPOSED POSITIONING ALGORITHM

Step no.	Operation
step 1	Estimate covariance matrix $\hat{\mathbf{R}}$ via (6).
step 2	Perform eigendecomposition on $\hat{\mathbf{R}}$ to obtain noise subspace $\mathbf{U}_n$.
step 3	Generate set of grid $\tilde{\mathbf{\Theta}}_1, \tilde{\mathbf{\Theta}}_2, \cdots, \tilde{\mathbf{\Theta}}_P$.
step 4	For each $\tilde{\mathbf{\Theta}}_p$ $(p = 1, 2, \cdots, P)$, construct $\mathbf{Q}(\tilde{\mathbf{\Theta}}_p)$ according to (15). Then calculate spectrum function in (24), or compute spectrum function in (28).
step 5	Obtain DOA by finding K peaks of spectrum function.
step 6	Obtain mutual coupling coefficients by (25).
step 7	Recover coordinates via (30).

TABLE II
DETAILED COMPLEXITY OF THE PROPOSED ALGORITHM

Step no.	Complexity
step 1	M^2L
step 2	$\mathrm{O}\{M^3\}$
step 4	$P\left(M^2Q + Q^2M + \mathrm{O}\{Q^3\}\right)$
step 6	K

IV. ALGORITHM ANALYSIS

A. Identifiability

According to Section III-A, the DOA is estimated using the rank reduction property of $\mathbf{Q}(\Theta)$. Since $\mathbf{Q}(\Theta) = \mathbf{T}^{\mathrm{H}}(\Theta)\mathbf{U}_n\mathbf{U}_n^{\mathrm{H}}\mathbf{T}(\Theta) \in \mathbb{C}^{Q\times Q}$, thus the maximum rank of $\mathbf{Q}(\Theta)$ is $\min\{Q, M-K\}$. If $Q > M-K$, then $\mathbf{Q}(\Theta)$ is the natural rank deficit, and the proposed algorithm will fail to work. Therefore, a sufficient condition of the proposed algorithm is $Q \leq M-K$, or equivalently, $K \leq M-Q$, which reveals that the maximum identifiability of the proposed algorithm is $M-Q$. Based on this assumption, the rank reduction of $\mathbf{Q}(\Theta)$ will take place in the estimation of Θ. If $K > M-Q$, then $\mathbf{Q}(\Theta)$ is natural singular, and no peak value will occur in (28), then the proposed algorithm will be invalid.

As pointed out in [54], the upper bound on Q is $M-K$; thus the proposed algorithm and iterative method in [54] have the same identifiability.

B. Computational Complexity

We analyze the complexity of the proposed method (by counting the number of complex multiplications), as shown in Table II. It can be observed that the dominant complexity of the proposed algorithm is the spectrum searching in step 4.

In [54], before the iteration, the same operation is required in steps 1 and 2. Each iteration in [54] has two parts, MUSIC spectrum searching and mutual coupling coefficient calculation, which require $P(2M^2+2M)$ and $M^2Q+Q^2M+K^2Q^3+KQ^3+O\{Q^3\}$ complex multiplications, respectively. Thus, the total complexity of the method in [54] is $M^2L + O\{M^3\} + W(P(2M^2+2M) + M^2Q + Q^2M + K^2Q^3 + KQ^3 + O\{Q^3\})$,

where W is the iteration number. Generally, dozens of iterations are required before convergence, and thus the proposed algorithm is computationally more efficient than the method in [54]. We will compare the complexity in Section V.

C. Deterministic CRBs

Performance bounds for wideband localization with commonly used signal metrics (such as TOA, TDOA, DOA, and RSS) were derived in [55] and [56]. The bounds for narrowband localization were stressed in [57], to which interested readers can refer for more details. Unlike prior work, we consider the scenario of DOA estimation for narrowband signals with unknown mutual coupling, and we derive the deterministic CRBs with respect to DOA and mutual coupling estimation. We start by rewriting (4) as

$$\mathbf{x}_l = \mathbf{C}\mathbf{A}\mathbf{s}_l + \mathbf{n}_l, \quad l = 1, 2, \ldots, L \tag{31}$$

where $\mathbf{x}_l \triangleq \mathbf{x}(l)$, $\mathbf{s}_l \triangleq \mathbf{s}(l)$, and $\mathbf{n}_l \triangleq \mathbf{n}(l)$. Thereafter, we construct a "column" measurement $\mathbf{y} = [\mathbf{x}_1^{\mathrm{T}}, \mathbf{x}_2^{\mathrm{T}}, \ldots, \mathbf{x}_L^{\mathrm{T}}]^{\mathrm{T}} \in \mathbb{C}^{ML\times 1}$. We assume that the source signals are deterministic but unknown to the receiver. Then, the mean $\mu \in \mathbb{C}^{ML\times 1}$ and covariance matrix $\Gamma \in \mathbb{C}^{ML\times ML}$ of the observed data are

$$\mu = \begin{bmatrix} \mathbf{C}\mathbf{A}\mathbf{s}_1 \\ \vdots \\ \mathbf{C}\mathbf{A}\mathbf{s}_L \end{bmatrix} = \mathbf{H}\mathbf{S} \tag{32a}$$

$$\Gamma = \mathrm{blkdiag}\{\underbrace{\sigma^2\mathbf{I}_M, \sigma^2\mathbf{I}_M, \ldots, \sigma^2\mathbf{I}_M}_{L}\}, \tag{32b}$$

where $\mathbf{H} \triangleq \mathrm{blkdiag}\{\underbrace{\mathbf{C}\mathbf{A}, \mathbf{C}\mathbf{A}, \ldots, \mathbf{C}\mathbf{A}}_{L}\} \in \mathbb{C}^{ML\times LK}$ and $\mathbf{S} \triangleq [\mathbf{s}_1^{\mathrm{T}}, \mathbf{s}_2^{\mathrm{T}}, \ldots, \mathbf{s}_L^{\mathrm{T}}]^{\mathrm{T}} \in \mathbb{C}^{LK\times 1}$.

Next, we define the parameter vectors $\theta \triangleq [\theta_1, \theta_2, \ldots, \theta_K]$, $\phi \triangleq [\phi_1, \phi_2, \ldots, \phi_K]$, $\alpha \triangleq [\theta, \varphi] \in \mathbb{R}^{1\times 2K}$, $\beta \triangleq [\mathrm{Re}\{\mathbf{c}\}, \mathrm{Im}\{\mathbf{c}\}] \in \mathbb{R}^{1\times 2Q}$, and $\gamma = [\mathrm{Re}\{\mathbf{S}^{\mathrm{T}}\}, \mathrm{Im}\{\mathbf{S}^{\mathrm{T}}\}] \in \mathbb{R}^{1\times 2LK}$. The entire estimation parameter vector is formulated as $\zeta = [\alpha, \beta, \gamma]^{\mathrm{T}}$. According to [58], the CRB matrix for ζ is given by

$$\mathrm{CRB} = \frac{\sigma_n^2}{2}\left[\mathrm{Re}\left\{\Psi^{\mathrm{H}}\Psi\right\}\right]^{-1} \tag{33}$$

where $\Psi = [(\partial\mu/\partial\alpha), (\partial\mu/\partial\beta), (\partial\mu/\partial\gamma)]$.

We now focus on each part of Ψ. It is straightforward to find

$$\frac{\partial\mu}{\partial\gamma} = \left[\mathbf{H}, j\mathbf{H}\right] \in \mathbb{C}^{ML\times 2LK}. \tag{34}$$

Moreover, we have $(\partial\mu/\partial\alpha) \triangleq [(\partial\mu/\partial\theta), (\partial\mu/\partial\varphi)] \triangleq [\mathbf{C}\Delta_\theta, \mathbf{C}\Delta_\phi] \in \mathbb{C}^{ML\times 2K}$ with

$$\Delta_\theta = \begin{bmatrix} \left(\frac{\partial\mathbf{a}(\Theta_1)}{\partial\theta_1}\right)s_{1,1} & \cdots & \left(\frac{\partial\mathbf{a}(\Theta_K)}{\partial\theta_K}\right)s_{K,1} \\ \vdots & \ddots & \vdots \\ \left(\frac{\partial\mathbf{a}(\Theta_1)}{\partial\theta_1}\right)s_{1,L} & \cdots & \left(\frac{\partial\mathbf{a}(\Theta_K)}{\partial\theta_K}\right)s_{K,L} \end{bmatrix} \tag{35a}$$

$$\Delta_\phi = \begin{bmatrix} \left(\frac{\partial\mathbf{a}(\Theta_1)}{\partial\phi_1}\right)s_{1,1} & \cdots & \left(\frac{\partial\mathbf{a}(\Theta_K)}{\partial\phi_K}\right)s_{K,1} \\ \vdots & \ddots & \vdots \\ \left(\frac{\partial\mathbf{a}(\Theta_1)}{\partial\phi_1}\right)s_{1,L} & \cdots & \left(\frac{\partial\mathbf{a}(\Theta_K)}{\partial\phi_K}\right)s_{K,L} \end{bmatrix} \tag{35b}$$

where $s_{k,l}$ is the kth element of $\mathbf{s}_l$. Similarly, we define $(\partial\mu/\partial\gamma) \triangleq \nabla \in \mathbb{C}^{ML\times 2Q}$ with

$$\nabla = \begin{bmatrix} \left(\frac{\partial\mathbf{C}}{\partial\mathbf{c}_1}\right)\mathbf{A}\mathbf{s}_1 & \cdots & \left(\frac{\partial\mathbf{C}}{\partial\mathbf{c}_Q}\right)\mathbf{A}\mathbf{s}_1 \\ \vdots & \ddots & \vdots \\ \left(\frac{\partial\mathbf{C}}{\partial\mathbf{c}_1}\right)\mathbf{A}\mathbf{s}_L & \cdots & \left(\frac{\partial\mathbf{C}}{\partial\mathbf{c}_Q}\right)\mathbf{A}\mathbf{s}_L \end{bmatrix} \otimes [1, j]. \tag{36}$$

Letting $\Delta \triangleq [\mathbf{C}\Delta_\theta, \mathbf{C}\Delta_\phi]$, $(\partial\mu/\partial\zeta^{\mathrm{T}}) = [\Delta, \nabla, \mathbf{H}, j\mathbf{H}]$. Furthermore, we can obtain

$$\mathbf{J} = \mathrm{Re}\left\{\Psi^{\mathrm{H}}\Psi\right\} = \mathrm{Re}\left\{\begin{bmatrix} \Delta^{\mathrm{H}} \\ \nabla^{\mathrm{H}} \\ \mathbf{H}^{\mathrm{H}} \\ -j\mathbf{H}^{\mathrm{H}} \end{bmatrix}\left[\Delta, \nabla, \mathbf{H}, j\mathbf{H}\right]\right\}. \tag{37}$$

Since we are only interested in the CRB with respect to DOA estimation and mutual coupling estimation, we will extract those counterparts from $\mathbf{J}$ by means of diagonalization. We define

$$\mathbf{P}_\Delta \triangleq \left(\mathbf{H}^{\mathrm{H}}\mathbf{H}\right)^{-1}\mathbf{H}^{\mathrm{H}}\Delta \in \mathbb{C}^{LK\times 2K} \tag{38a}$$

$$\mathbf{P}_\nabla \triangleq \left(\mathbf{H}^{\mathrm{H}}\mathbf{H}\right)^{-1}\mathbf{H}^{\mathrm{H}}\nabla \in \mathbb{C}^{LK\times 2Q}. \tag{38b}$$

As $\mathbf{H}^{\mathrm{H}}\mathbf{H}$ is nonsingular, both $\mathbf{P}_\nabla^{-1}$ and $\mathbf{P}_\nabla^{-1}$ are valid. In addition, we define

$$\mathbf{V} \triangleq \begin{bmatrix} \mathbf{I} & \mathbf{0} & \mathbf{0} & \mathbf{0} \\ \mathbf{0} & \mathbf{I} & \mathbf{0} & \mathbf{0} \\ \text{-Re}\{\mathbf{P}_\Delta\} & \text{-Re}\{\mathbf{P}_\nabla\} & \mathbf{I} & \mathbf{0} \\ \text{-Im}\{\mathbf{P}_\Delta\} & \text{-Im}\{\mathbf{P}_\nabla\} & \mathbf{0} & \mathbf{I} \end{bmatrix}. \tag{39}$$

It is easy to find

$$\left[\Delta, \nabla, \mathbf{H}, j\mathbf{H}\right]\mathbf{V} = \left[(\Delta - \mathbf{H}\mathbf{P}_\Delta), (\nabla - \mathbf{H}\mathbf{P}_\nabla), \mathbf{H}, j\mathbf{H}\right]. \tag{40}$$

We let $\Pi_{\mathbf{H}}^{\perp}$ be the orthogonal projection of $\mathbf{H}^{\mathrm{H}}$ onto null space, i.e.,

$$\Pi_{\mathbf{H}}^{\perp} \triangleq \mathbf{I}_{ML} - \mathbf{H}\left(\mathbf{H}^{\mathrm{H}}\mathbf{H}\right)^{-1}\mathbf{H}^{\mathrm{H}}. \tag{41}$$

Obviously, $\mathbf{H}^{\mathrm{H}}\Pi_{\mathbf{H}}^{\perp} = \mathbf{0}$. Then, we have

$$\begin{aligned} \mathbf{V}^{\mathrm{H}}\mathbf{J}\mathbf{V} &= \mathrm{Re}\left\{\begin{bmatrix} \Delta^{\mathrm{H}}\Pi_{\mathbf{H}}^{\perp} \\ \nabla^{\mathrm{H}}\Pi_{\mathbf{H}}^{\perp} \\ \mathbf{H}^{\mathrm{H}} \\ -j\mathbf{H}^{\mathrm{H}} \end{bmatrix}\left[\Pi_{\mathbf{H}}^{\perp}\Delta, \Pi_{\mathbf{H}}^{\perp}\nabla, \mathbf{H}, j\mathbf{H}\right]\right\} \\ &= \mathrm{Re}\left\{\begin{bmatrix} \Delta_1 & \Delta_2 & \mathbf{0} & \mathbf{0} \\ \Delta_3 & \Delta_4 & \mathbf{0} & \mathbf{0} \\ \mathbf{0} & \mathbf{0} & \tilde{\mathbf{H}} & j\tilde{\mathbf{H}} \\ \mathbf{0} & \mathbf{0} & -j\tilde{\mathbf{H}} & \tilde{\mathbf{H}} \end{bmatrix}\right\} \end{aligned} \tag{42}$$

with

$$\Delta_1 = \Delta^{\mathrm{H}}\Pi_{\mathbf{H}}^{\perp}\Delta \tag{43a}$$

$$\Delta_2 = \Delta^{\mathrm{H}}\Pi_{\mathbf{H}}^{\perp}\nabla \tag{43b}$$

$$\Delta_3 = \nabla^{\mathrm{H}}\Pi_{\mathbf{H}}^{\perp}\Delta \tag{43c}$$

$$\Delta_4 = \nabla^{\mathrm{H}}\Pi_{\mathbf{H}}^{\perp}\nabla \tag{43d}$$

$$\tilde{\mathbf{H}} = \mathbf{H}^{\mathrm{H}}\mathbf{H}. \tag{43e}$$

According to properties of a partitioned diagonal matrix, we obtain

$$\begin{aligned}\mathbf{J}^{-1} &= \mathbf{V}\left(\mathbf{V}^{\mathrm{H}}\mathbf{J}\mathbf{V}\right)^{-1}\mathbf{V}^{\mathrm{T}} \\ &= \begin{bmatrix}\mathbf{I} & \mathbf{0} & \mathbf{0}\\ \mathbf{0} & \mathbf{I} & \mathbf{0}\\ \times & \times & \mathbf{I}\end{bmatrix}\cdot\begin{bmatrix}\mathrm{Re}\{\Delta_1\} & \mathrm{Re}\{\Delta_2\} & \mathbf{0}\\ \mathrm{Re}\{\Delta_3\} & \mathrm{Re}\{\Delta_4\} & \mathbf{0}\\ \mathbf{0} & \mathbf{0} & \times\end{bmatrix}^{-1} \\ &\quad\times\begin{bmatrix}\mathbf{I} & \mathbf{0} & \times\\ \mathbf{0} & \mathbf{I} & \times\\ \mathbf{0} & \mathbf{0} & \mathbf{I}\end{bmatrix} \\ &= \begin{bmatrix}\mathrm{Re}\{\Delta_1\} & \mathrm{Re}\{\Delta_2\} & \mathbf{0}\\ \mathrm{Re}\{\Delta_3\} & \mathrm{Re}\{\Delta_4\} & \mathbf{0}\\ \mathbf{0} & \mathbf{0} & \times\end{bmatrix}^{-1}\end{aligned} \tag{44}$$

where $\times$ denotes the irrelevant part in the derivation. Inserting (37) and (44) into (33), and removing all the unaffected parts, we can then obtain the CRBs on DOA estimation and mutual coupling estimation as

$$\mathrm{CRB}_{a,c} = \frac{\sigma^2}{2}\begin{bmatrix}\mathrm{Re}\{\Delta_1\} & \mathrm{Re}\{\Delta_2\}\\ \mathrm{Re}\{\Delta_3\} & \mathrm{Re}\{\Delta_4\}\end{bmatrix}^{-1}. \tag{45}$$

According to the inverse property of a partitioned matrix, we can obtain the CRB on DOA estimation CRB_d and the CRB on mutual coupling estimation CRB_m, respectively, as

$$\mathrm{CRB}_d = \frac{\sigma^2}{2}\left[\mathrm{Re}\{\Delta_1\} - \mathrm{Re}\{\Delta_2\}\mathrm{Re}^{-1}\{\Delta_4\}\mathrm{Re}\{\Delta_3\}\right]^{-1} \tag{46a}$$

$$\mathrm{CRB}_m = \frac{\sigma^2}{2}\left[\mathrm{Re}\{\Delta_4\} - \mathrm{Re}\{\Delta_3\}\mathrm{Re}^{-1}\{\Delta_1\}\mathrm{Re}\{\Delta_2\}\right]^{-1}. \tag{46b}$$

In this article, the CRB is adopted to evaluate the theoretical lower bound for each vehicle terminal. In practice, the positioning accuracy can be improved further by network localization and navigation (NLN) [59], [60], which advocates that agents jointly infer their states. The NLN exploits joint spatial and temporal cooperation for position inference.

V. Simulation Results

To show the efficiency of our method, Monte Carlo trials were carried out. In the simulations, we assumed that there are M sensors and K far-field sources. The source signals satisfied a normal distribution, and $L = 200$ snapshots were collected. The signal-to-noise ratio (SNR) in the simulation is defined as $\mathrm{SNR} \triangleq 10\log_{10}\|\mathbf{x}(t) - \mathbf{n}(t)\|_F^2/\|\mathbf{n}(t)\|_F^2$ [dB]. All the simulations were run on an HP Z840 workstation [two Intel Xeon E5-2650 v4 2.20-GHz processors with 128-GB DDR4 RAM) with MATLAB R2016a (MathWorks, USA). Two metrics were adopted for performance assessment. One is the root-mean-square error (RMSE); and the other is the runtime. The RMSE is defined as

$$\mathrm{RMSE} = \frac{1}{K}\sum_{k=1}^{K}\sqrt{\frac{1}{T}\sum_{i=1}^{\mathrm{T}}\left(\hat{\zeta}_{i,k} - \zeta_k\right)^2} \tag{47}$$

where T is the total number of trails, and ζ_k and $\hat{\zeta}_{i,k}$ are the kth parameter (angle or mutual coupling coefficient) and its estimate, respectively, for the ith Monte Carlo trial. Two array geometries were considered.

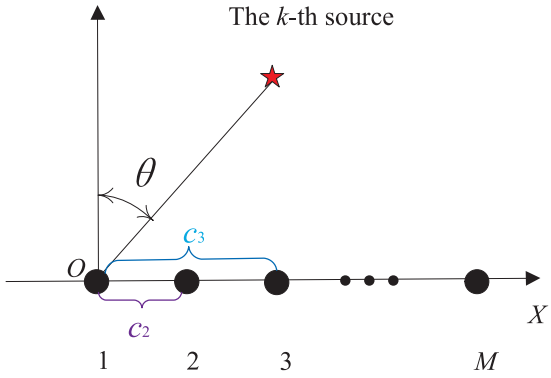

Fig. 3. Illustration of ULA.

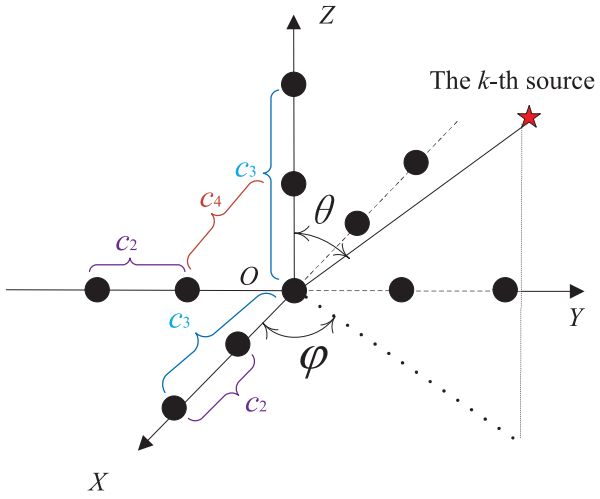

Fig. 4. Illustration of 3D-ULA.

Scenario 1: ULA geometry with interelement distance of $\lambda/2$, as shown in Fig. 3. We assumed $Q = 3$ and $\mathbf{c} = [1, 0.8 + 0.5j, 0.2 + 0.1j]^{\mathrm{T}}$. In such a case, we only needed to estimate the azimuth angle θ.

Scenario 2: 3D-ULA with $M = 12$ and interelement distance of $\lambda/2$, as shown in Fig. 4, again assuming $Q = 3$. The mutual coefficient between two adjacent sensors was $c_2 = 0.8 + 0.5j$, and the mutual coupling coefficient between sensors with distance λ was $c_3 = 0.017 + 0.035j$, while the mutual coefficient associated with two cross-adjacent sensors was $c_4 = 0.2 + 0.1j$. Therefore, $Q = 4$ and $\mathbf{c} = [1, 0.8 + 0.5j, 0.017 + 0.035j, 0.2 + 0.1j]^{\mathrm{T}}$. In addition, we assumed $K = 2$ sources located at $\Theta = (40°, 25°)$ and $\Theta = (60°, 105°)$, respectively.

In the first example, we illustrate the spatial spectrum of the proposed algorithm in scenario 1. We assume that $M = 12$, SNR = 20 dB, and $K = 3$ with DOAs are 20°, 25°, and 40°, respectively. The search range of all of the algorithms was [0°, 90°] with interval 0.1°. For comparison, the spectrum obtained by MUSIC (marked with "MUSIC") and the iterative method in [54] (marked with "iterative method") are added (all the compared algorithms share the same simulation parameters). For each algorithm, five independent trials were run. The result is depicted in Fig. 5, from which we can observe that the traditional MUSIC could only obtain two DOAs. However, both the proposed algorithm and the

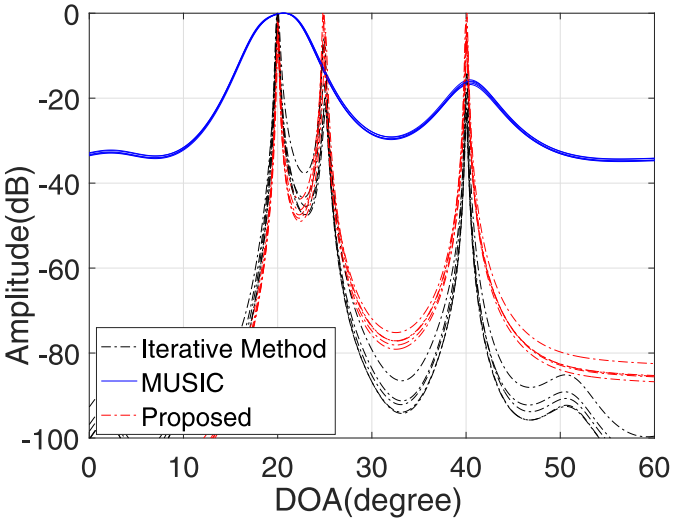

Fig. 5. Spectrum comparison in scenario 1.

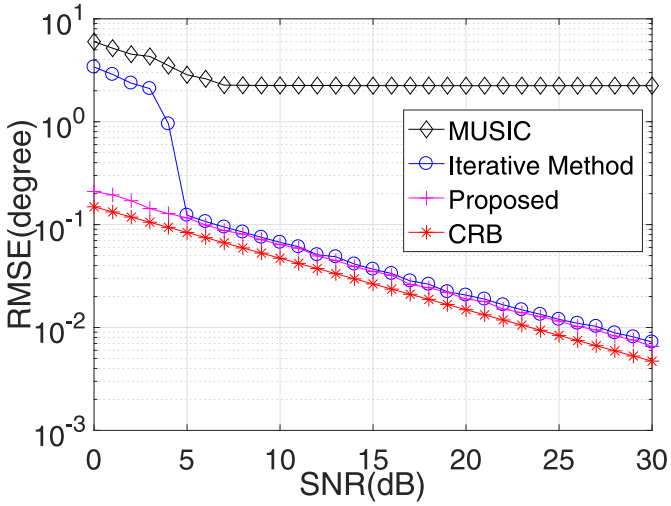

Fig. 7. RMSE for DOA estimation versus SNR in scenario 1.

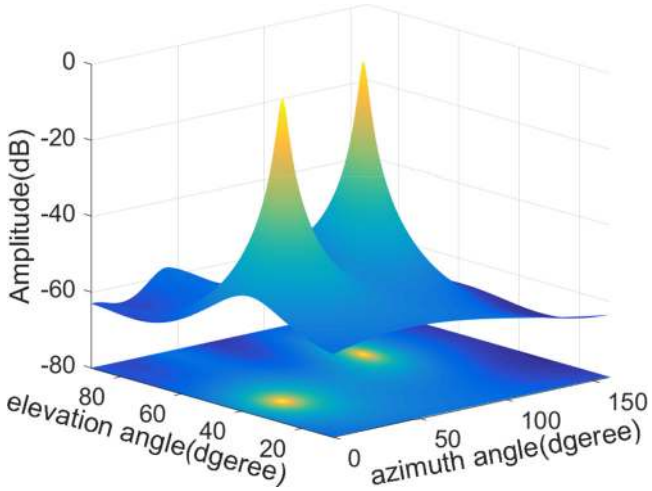

Fig. 6. Spectrum result of the proposed algorithm in scenario 2.

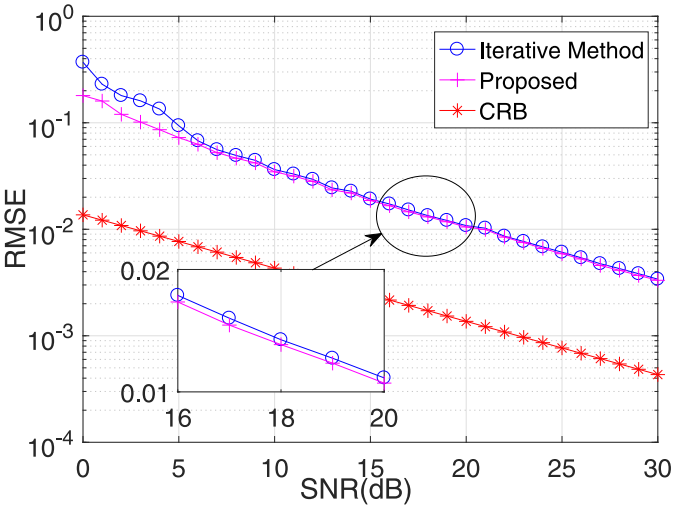

Fig. 8. RMSE for mutual coupling estimation versus SNR in scenario 1.

iterative method offered good performance, since they were robust enough against mutual coupling.

In the second example, we tested the performance of the proposed algorithm in scenario 2, where SNR= 10 dB was considered. The search range for θ was $[0°, 90°]$ with interval 0.5°, while the search range for ϕ was $[0°, 180°]$ with interval 1°. The spatial spectrum result is illustrated in Fig. 6. Clearly, the proposed algorithm could correctly detect and pair the 2D-DOAs.

In the third example, we measured the estimation performance of the proposed algorithm in the presence of scenario 1, where $M = 12$ and $K = 2$, with DOAs are 20° and 30°, respectively. The search range was $[0°, 90°]$, with interval 0.01°. The curves of RMSE versus SNR are shown in Figs. 7 and 8 (the performance of MUSIC is not shown in Fig. 8, as it cannot offer mutual coupling estimation). The RMSEs of the proposed and iterative methods seem almost identical except for some low SNR cases. For the proposed algorithm, DOA estimation accuracy is only related to SNR, while in the iterative method, it is related to both SNR, but also relate to and the estimation accuracy of the mutual coupling coefficient. The estimation error in the iterative method has a cumulative effect. As a result, the proposed method would perform better than the iterative method in low SNR regions. However, the advantage is not obvious for mutual coupling coefficient estimation, as shown in Fig. 8. There is a big gap between the estimation performance and the theoretical bound, hence more work is necessary to solve this problem. Fig. 9 shows that the average runtime of the proposed algorithm is about an order of magnitude lower than that of the iterative method, which implies that the proposed algorithm is more efficient.

In the fourth example, we repeated the simulation in scenario 2. The search range for θ was $[20°, 80°]$, with interval 0.2°, while the search range for ϕ was $[0°, 130°]$, with the interval set to 0.5°. The RMSE curves for DOA estimation are shown in Fig. 10, and those for the RMSE curves for mutual coupling estimation are given in Fig. 11. It is clearly seen that RMSE of the traditional MUSIC algorithm barely changed in such a scenario, while RMSE of the proposed

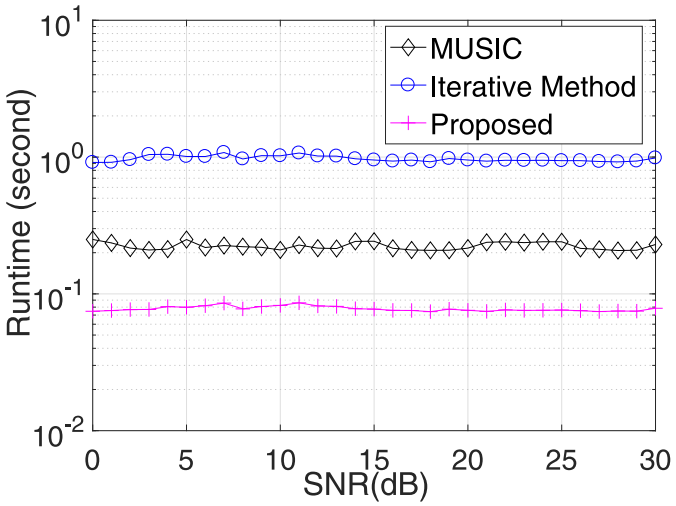

Fig. 9. Average runtime versus SNR in scenario 1.

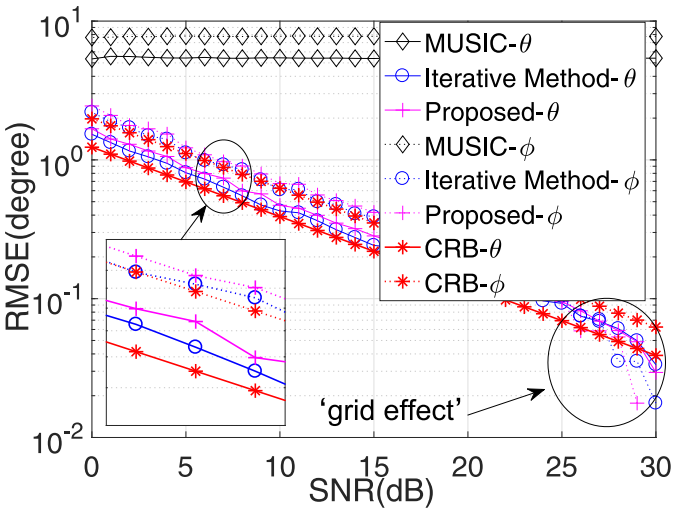

Fig. 10. RMSE for DOA estimation versus SNR in scenario 2.

algorithm would decrease with the increasing SNR. Moreover, the proposed algorithm and the iterative method had similar estimation performance, and both attained the CRB. The runtime results, as illustrated in Fig. 12, indicate that the average runtime of the iterative method was about three times that the proposed algorithm. Therefore, the proposed algorithm is much more efficient.

In the fifth example, we compared the performance with various sensor numbers M in scenario 1, with the SNR fixed at 10 dB, and the other conditions are the same as that in the third example. Figs. 13 and 14, respectively, present the RMSE on DOA estimation and mutual coupling estimation. One can observe that the RMSE on DOA estimation slowly decreased with increasing M, while the RMSE on mutual coupling estimation barely changed with various M values. In addition, it appears that the proposed algorithm performed better than the iterative method. Fig. 15 shows the average runtime comparison. Noteworthy is that the proposed algorithm was computationally more efficient than the iterative method. As mentioned previously, the method in [54] involves

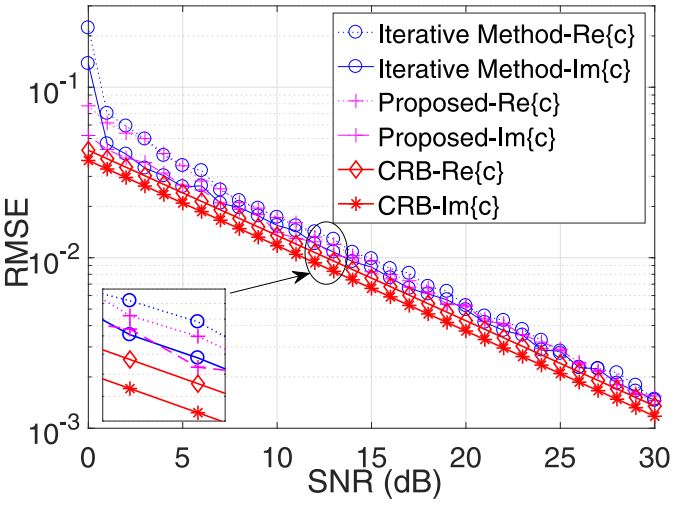

Fig. 11. RMSE for mutual coupling estimation versus SNR in scenario 2.

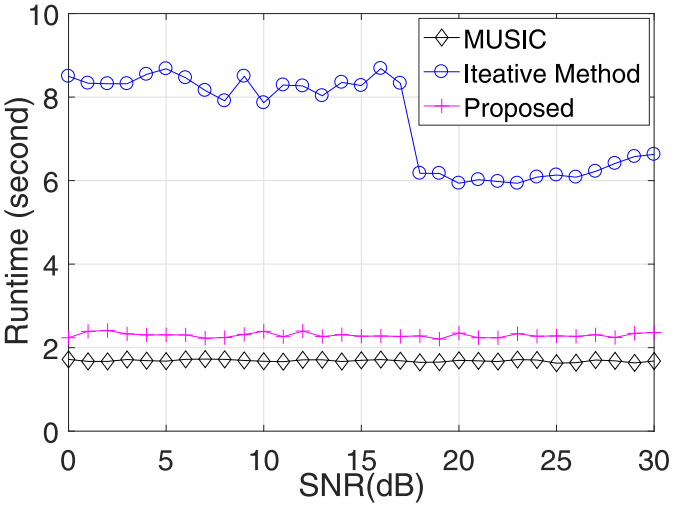

Fig. 12. Average runtime versus SNR in scenario 2.

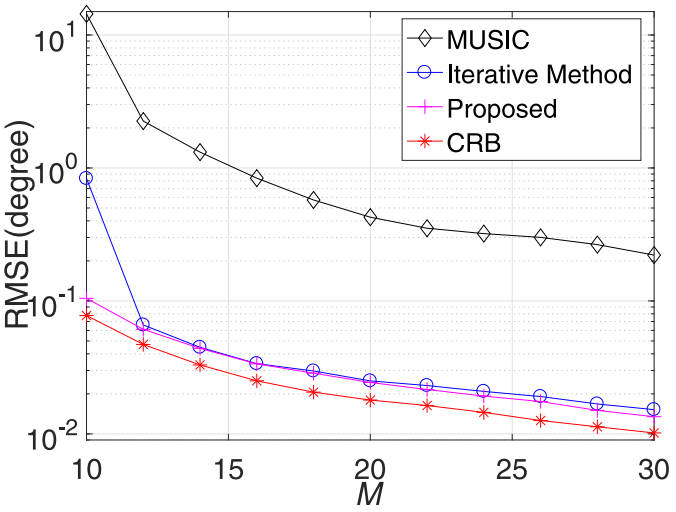

Fig. 13. RMSE for DOA estimation versus M in scenario 1.

optimization of a highly nonlinear problem and, more significantly, an iterative procedure, which is time consuming. In contrast, the proposed algorithm only needs a peak search process.

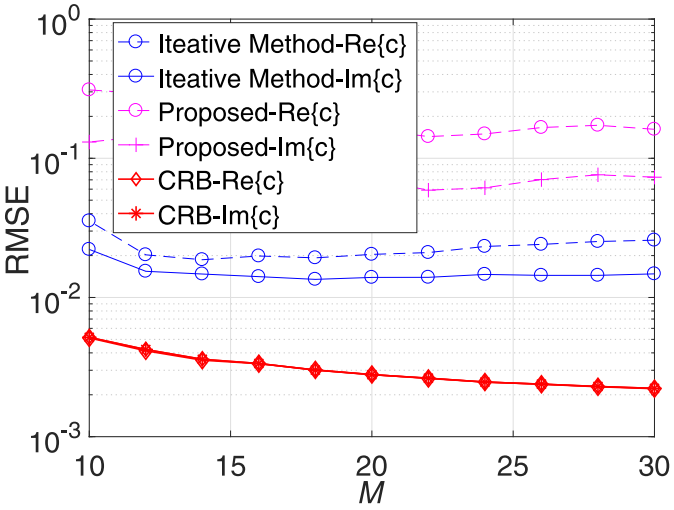

Fig. 14. RMSE for mutual coefficient estimation versus M in scenario 1.

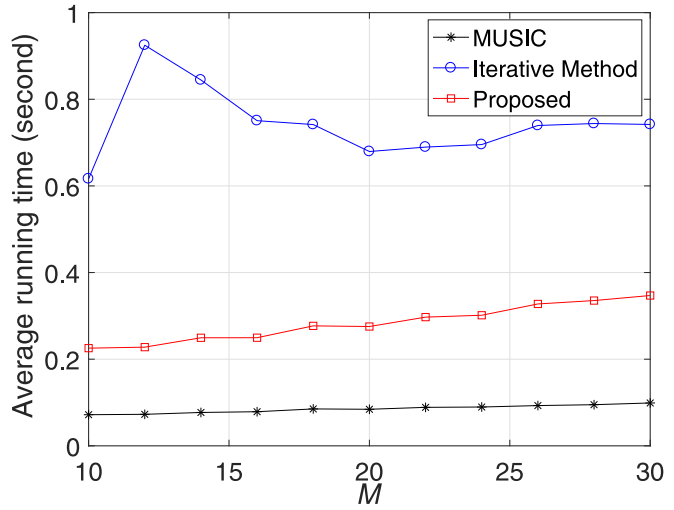

Fig. 15. Average runtime versus M in scenario 1.

TABLE III
VEHICLE POSITIONING RESULTS USING 1D-DOA ESTIMATION

SNR (dB)	Absolute error (m)		
	MUSIC	Iterative Method	Proposed
0	50.67	35.09	1.61
5	24.09	7.03	0.90
10	18.08	0.50	0.46
15	18.08	0.29	0.27
20	18.08	0.17	0.15

Finally, the vehicle positioning performance of different DOA estimation algorithms was tested relying on the proposed auxiliary vehicle positioning framework. First, we considered scenario 1, in which the positions of the landmarks were (0, 0) and (0, 50 m). We then considered scenario 2 with landmarks located at (0, 0, 0) and (0, 50 m, 10 m). Theoretically, the coordinates of the vehicle with respect to the two scenarios were (234.32 m, −85.29 m) and (20.80 m, −30.71 m, 36.60 m), respectively. Tables III and IV compare the vehicle positioning performance in scenario 1 and scenario 2, respectively. It is seen that the traditional MUSIC algorithm was not suitable

TABLE IV
VEHICLE POSITIONING RESULTS USING 2D-DOA ESTIMATION

SNR (dB)	Absolute error (m)		
	MUSIC	Iterative Method	Proposed
0	21.60	5.85	6.64
5	21.60	3.19	3.73
10	21.60	1.73	1.89
15	21.60	0.96	1.04
20	21.60	0.55	0.61

for accurate vehicle positioning in either scenario, since its absolute error was too large. In scenario 1, the proposed DOA estimation algorithm achieved better positioning performance than that of the iterative method. Moreover, it was more robust than the latter in low SNR regions. In scenario 2, the method in [54] performed slightly better than the proposed algorithm.

VI. CONCLUSION

In this article, we proposed an auxiliary vehicle positioning framework that relies on robust DOA estimation within current VANETs. We considered a realistic scenario in which sensors are irregularly distributed in a vehicle, and they suffer from the mutual coupling. We derived a computationally friendly algorithm for DOA estimation and mutual coupling self-calibration in such a scenario. By utilizing the RD-MUSIC idea, the proposed algorithm can obtain the DOA and mutual coupling coefficient by searching a single spatial spectrum. The proposed algorithm has estimation performance that is very close to the state-of-the-art iterative method, but it is superior from an engineering standpoint, since it is much more efficient. Simulation experiments corroborate our theoretical analysis. The proposed positioning framework can provide a self-localization service, and it can collaborate with other positioning systems; thus it should have bright prospects for future IoV applications.

ACKNOWLEDGMENT

MATLAB codes are available on our website with security code k7mg.

REFERENCES

[1] H. Peng, L. Liang, X. Shen, and G. Y. Li, "Vehicular communications: A network layer perspective," *IEEE Trans. Veh. Technol.*, vol. 68, no. 2, pp. 1064–1078, Feb. 2019.
[2] K. Guan *et al.*, "5-GHz obstructed vehicle-to-vehicle channel characterization for Internet of intelligent vehicles," *IEEE Internet Things J.*, vol. 6, no. 1, pp. 100–110, Feb. 2019.
[3] Q. Yuan, H. Zhou, Z. Liu, J. Li, F. Yang, and X. Shen, "CESense: Cost-effective urban environment sensing in vehicular sensor networks," *IEEE Trans. Intell. Transp. Syst.*, vol. 20, no. 9, pp. 3235–3246, Sep. 2019.
[4] F. Tang, B. Mao, Z. M. Fadlullah, J. Liu, and N. Kato, "ST-DeLTA: An novel spatial–temporal value network aided deep learning based intelligent network traffic control system," *IEEE Trans. Sustain. Comput.*, vol. 20, no. 9, pp. 3235–3246, Sep. 2019.
[5] N. Cheng *et al.*, "Space/aerial-assisted computing offloading for IoT applications: A learning-based approach," *IEEE J. Sel. Area. Commun.*, vol. 37, no. 5, pp. 1117–1129, May 2019.
[6] W. Wu, N. Zhang, N. Cheng, Y. Tang, K. Aldubaikhy, and X. Shen, "Beef up mmWave dense cellular networks with D2D-assisted cooperative edge caching," *IEEE Trans. Veh. Technol.*, vol. 68, no. 4, pp. 3890–3904, Apr. 2019.

[7] T. Jiang, H. Fang, and H. Wang, "Blockchain-based Internet of Vehicles: Distributed network architecture and performance analysis," *IEEE Internet Things J.*, vol. 6, no. 3, pp. 4640–4649, Jun. 2019.

[8] W. Xu, S. Wang, S. Yan, and J. He, "An efficient wideband spectrum sensing algorithm for unmanned aerial vehicle communication networks," *IEEE Internet Things J.*, vol. 6, no. 2, pp. 1768–1780, Apr. 2019.

[9] Z. Zhang, H. Wu, H. Zhang, H. Dai, and N. Kato, "Virtual-MIMO-boosted information propagation on highways," *IEEE Trans. Wireless Commun.*, vol. 15, no. 2, pp. 1420–1431, Feb. 2016.

[10] H. Huang, J. Yang, Y. Song, H. Huang, and G. Gui, "Deep learning for super-resolution channel estimation and DOA estimation based massive MIMO system," *IEEE Trans. Veh. Technol.*, vol. 67, no. 9, pp. 8549–8560, Sep. 2018.

[11] H. Huang, Y. Song, J. Yang, G. Gui, and F. Adachi, "Deep-learning-based millimeter-wave massive MIMO for hybrid precoding," *IEEE Trans. Veh. Technol.*, vol. 68, no. 3, pp. 3027–3032, Mar. 2019.

[12] N. Kato *et al.*, "Optimizing space-air-ground integrated networks by artificial intelligence," *IEEE Wireless Commun.*, vol. 26, no. 4, pp. 140–147, Aug. 2019.

[13] Y. Wang, M. Liu, J. Yang, and G. Gui, "Data-driven deep learning for automatic modulation recognition in cognitive radios," *IEEE Trans. Veh. Technol.*, vol. 68, no. 4, pp. 4074–4077, Apr. 2019.

[14] G. Gui, H. Huang, Y. Song, and H. Sari, "Deep learning for an effective nonorthogonal multiple access scheme," *IEEE Trans. Veh. Technol.*, vol. 67, no. 9, pp. 8440–8450, Sep. 2018.

[15] F. Tang, Z. M. Fadlullah, B. Mao, and N. Kato, "An intelligent traffic load prediction-based adaptive channel assignment algorithm in SDN-IoT: A deep learning approach," *IEEE Internet Things J.*, vol. 5, no. 6, pp. 5141–5154, Dec. 2018.

[16] L. Wan, L. Sun, X. Kong, Y. Yuan, K. Sun, and F. Xia, "Task-driven resource assignment in mobile edge computing exploiting evolutionary computation," *IEEE Wireless Commun.*, vol. 26, no. 6, pp. 94–101, Dec. 2019.

[17] Y. Wang, J. Yang, M. Liu, and G. Gui, "LightAMC: Lightweight automatic modulation classification using deep learning and compressive sensing," *IEEE Trans. Veh. Technol.*, vol. 69, no. 3, pp. 3491–3495, Mar. 2020.

[18] A. Conti, S. Mazuelas, S. Bartoletti, W. C. Lindsey, and M. Z. Win, "Soft information for localization-of-things," *Proc. IEEE*, vol. 107, no. 11, pp. 2240–2264, Nov. 2019.

[19] S. Kuutti, S. Fallah, K. Katsaros, M. Dianati, F. Mccullough, and A. Mouzakitis, "A survey of the state-of-the-art localization techniques and their potentials for autonomous vehicle applications," *IEEE Internet Things J.*, vol. 5, no. 2, pp. 829–846, Apr. 2018.

[20] G. Soatti, M. Nicoli, N. Garcia, B. Denis, R. Raulefs, and H. Wymeersch, "Implicit cooperative positioning in vehicular networks," *IEEE Trans. Intell. Transp. Syst.*, vol. 19, no. 12, pp. 3964–3980, Dec. 2018.

[21] H. Zhu, K. Yuen, L. Mihaylova, and H. Leung, "Overview of environment perception for intelligent vehicles," *IEEE Trans. Intell. Transp. Syst.*, vol. 18, no. 10, pp. 2584–2601, Oct. 2017.

[22] I. Bisio, F. Lavagetto, M. Marchese, and A. Sciarrone, "Energy efficient WiFi-based fingerprinting for indoor positioning with smartphones," in *Proc. IEEE Global Commun. Conf. (GLOBECOM)*, Dec. 2013, pp. 4639–4643.

[23] J. P. Beaudeau, M. F. Bugallo, and P. M. Djuri, "RSSI-based multi-target tracking by cooperative agents using fusion of cross-target information," *IEEE Trans. Signal Process.*, vol. 63, no. 19, pp. 5033–5044, Oct. 2015.

[24] D. Oh and J. Lee, "Robust super-resolution TOA estimation against doppler shift for vehicle tracking," *IEEE Commun. Lett.*, vol. 18, no. 5, pp. 745–748, May 2014.

[25] H. Jamali-Rad and G. Leus, "Sparsity-aware multi-source TDOA localization," *IEEE Trans. Signal Process.*, vol. 61, no. 19, pp. 4874–4887, Oct. 2013.

[26] B. Huang, L. Xie, and Z. Yang, "TDOA-based source localization with distance-dependent noises," *IEEE Trans. Wireless Commun.*, vol. 14, no. 1, pp. 468–480, Jan. 2015.

[27] A. Saucan, T. Chonavel, C. Sintes, and J. Le Caillec, "CPHD-DOA tracking of multiple extended sonar targets in impulsive environments," *IEEE Trans. Signal Process.*, vol. 64, no. 5, pp. 1147–1160, Mar. 2016.

[28] H. Wang, L. Wan, M. Dong, K. Ota, and X. Wang, "Assistant vehicle localization based on three collaborative base stations via SBL-based robust DOA estimation," *IEEE Internet Things J.*, vol. 6, no. 3, pp. 5766–5777, Jun. 2019.

[29] H. Wymeersch, G. Seco-Granados, G. Destino, D. Dardari, and F. Tufvesson, "5G mmWave positioning for vehicular networks," *IEEE Wireless Commun.*, vol. 24, no. 6, pp. 80–86, Dec. 2017.

[30] Z. Abu-Shaban, X. Zhou, T. Abhayapala, G. Seco-Granados, and H. Wymeersch, "Error bounds for uplink and downlink 3D localization in 5G millimeter wave systems," *IEEE Wireless Commun.*, vol. 17, no. 8, pp. 4939–4954, Aug. 2018.

[31] Y. Wang, Y. Wu, and Y. Shen, "Joint spatiotemporal multipath mitigation in large-scale array localization," *IEEE Trans. Signal Process.*, vol. 67, no. 3, pp. 783–797, Feb. 2019.

[32] F. Wen, J. Shi, and Z. Zhang, "Direction finding for bistatic MIMO radar with unknown spatially colored noise," *Circuit Syst. Signal Process.*, to be published, doi: 10.1007/s00034-019-01260-5.

[33] X. Wang, L. Wan, M. Huang, C. Shen, Z. Han, and T. Zhu, "Low-complexity channel estimation for circular and noncircular signals in virtual MIMO vehicle communication systems," *IEEE Trans. Veh. Technol.*, early access, doi: 10.1109/TVT.2020.2970967.

[34] F. Wen, C. Mao, and G. Zhang, "Direction finding in MIMO radar with large antenna arrays and nonorthogonal waveforms," *Digit. Signal Process.*, vol. 94, pp. 75–83, Nov. 2019.

[35] B. Liao, "Fast angle estimation for MIMO radar with nonorthogonal waveforms," *IEEE Trans. Aerosp. Electron. Syst.*, vol. 54, no. 4, pp. 2091–2096, Aug. 2018.

[36] F. Wen, J. Shi, and Z. Zhang, "Joint 2D-DOD, 2D-DOA and polarization angles estimation for bistatic EMVS-MIMO radar via PARAFAC analysis," *IEEE Trans. Veh. Technol.*, vol. 69, no. 2, pp. 1626–1638, Feb. 2020.

[37] B. Wang, Y. Wang, and Y. Guo, "Mutual coupling calibration with instrumental sensors," *Electron. Lett.*, vol. 40, no. 7, pp. 406–408, Apr. 2004.

[38] B. Friedlander and A. J. Weiss, "Direction finding in the presence of mutual coupling," *IEEE Trans. Antennas Propag.*, vol. 39, no. 3, pp. 273–284, Mar. 1991.

[39] B. Liao, Z. Zhang, and S. Chan, "DOA estimation and tracking of ULAs with mutual coupling," *IEEE Trans. Aerosp. Electron. Syst.*, vol. 48, no. 1, pp. 891–905, Jan. 2012.

[40] Z. Liu and Y. Zhou, "A unified framework and sparse Bayesian perspective for direction-of-arrival estimation in the presence of array imperfections," *IEEE Trans. Signal Process.*, vol. 61, no. 15, pp. 3786–3798, Aug. 2013.

[41] P. Chen, Z. Cao, Z. Chen, and X. Wang, "Off-grid DOA estimation using sparse Bayesian learning in MIMO radar with unknown mutual coupling," *IEEE Trans. Signal Process.*, vol. 67, no. 1, pp. 208–220, Jan. 2019.

[42] D. Meng, X. Wang, M. Huang, and C. Shen, "Reweighted l_1l1-norm minimisation for high-resolution DOA estimation under unknown mutual coupling," *Electron. Lett.*, vol. 54, no. 23, pp. 1346–1348, Nov. 2018.

[43] Y. Wang, L. Wang, J. Xie, M. Trinkle, and B. W.-H. Ng, "DOA estimation under mutual coupling of uniform linear arrays using sparse reconstruction," *IEEE Wireless Commun. Lett.*, vol. 8, no. 4, pp. 1004–1007, Aug. 2019.

[44] J. Xie, L. Wang, and J. Su, "Efficient DOA estimation algorithm for noncircular sources under unknown mutual coupling," *IEEE Sensors Lett.*, vol. 2, no. 3, pp. 1–4, Sep. 2018.

[45] J. Xie, L. Wang, and Y. Wang, "Efficient real-valued rank reduction algorithm for DOA estimation of noncircular sources under mutual coupling," *IEEE Access*, vol. 6, pp. 64450–64460, 2018.

[46] H. S. Mir, "A generalized transfer-function based array calibration technique for direction finding," *IEEE Trans. Signal Process.*, vol. 56, no. 2, pp. 851–855, Feb. 2008.

[47] A. M. Elbir, "Calibration of directional mutual coupling for antenna arrays," *Digit. Signal Process.*, vol. 69, pp. 117–126, Oct. 2017.

[48] M. Lin and L. Yang, "Blind calibration and DOA estimation with uniform circular arrays in the presence of mutual coupling," *IEEE Trans. Antennas Propag.*, vol. 5, no. 1, pp. 315–318, Jul. 2006.

[49] R. Goossens and H. Rogier, "A hybrid UCA-RARE/Root-MUSIC approach for 2-D direction of arrival estimation in uniform circular arrays in the presence of mutual coupling," *IEEE Trans. Antennas Propag.*, vol. 55, no. 3, pp. 841–849, Mar. 2007.

[50] M. Wang, X. Ma, S. Yan, and C. Hao, "An autocalibration algorithm for uniform circular array with unknown mutual coupling," *IEEE Trans. Antennas Propag.*, vol. 15, pp. 12–15, Apr. 2016.

[51] Z. Ye and C. Liu, "2-D DOA estimation in the presence of mutual coupling," *IEEE Trans. Antennas Propag.*, vol. 56, no. 10, pp. 3150–3158, Oct. 2008.

[52] H. Wu, C. Hou, H. Chen, W. Liu, and Q. Wang, "Direction finding and mutual coupling estimation for uniform rectangular arrays," *Signal Process.*, vol. 117, pp. 61–68, Dec. 2015.

[53] J. Zhang, C. Hui, W. Huang, and W. Liu, "Self-calibration of mutual coupling for non-uniform cross-array," *Circuits Syst. Signal Process.*, vol. 38, no. 3, pp. 1137–1156, Jul. 2018.
[54] A. M. Elbir, "A novel data transformation approach for DOA estimation with 3-D antenna arrays in the presence of mutual coupling," *IEEE Antennas Wireless Propag. Lett.*, vol. 16, pp. 2118–2121, 2017.
[55] M. Z. Win, Y. Shen, and W. Dai, "A theoretical foundation of network localization and navigation," *Proc. IEEE*, vol. 106, no. 7, pp. 1136–1165, Jul. 2018.
[56] Y. Shen and M. Z. Win, "On the accuracy of localization systems using wideband antenna arrays," *IEEE Trans. Commun.*, vol. 58, no. 1, pp. 270–280, Jan. 2010.
[57] Y. Han, Y. Shen, X. Zhang, M. Z. Win, and H. Meng, "Performance limits and geometric properties of array localization," *IEEE Trans. Inf. Theory*, vol. 62, no. 2, pp. 1054–1075, Feb. 2016.
[58] P. Stoica and A. Nehorai, "Performance study of conditional and unconditional direction-of-arrival estimation," *IEEE Trans. Acoust., Speech, Signal Process.*, vol. 38, no. 10, pp. 1783–1795, Oct. 1990.
[59] Y. Shen and M. Z. Win, "Fundamental limits of wideband localization—Part I: A general framework," *IEEE Trans. Inf. Theory*, vol. 56, no. 10, pp. 4956–4980, Oct. 2010.
[60] Y. Shen, H. Wymeersch, and M. Z. Win, "Fundamental limits of wideband localization—Part II: Cooperative networks," *IEEE Trans. Inf. Theory*, vol. 56, no. 10, pp. 4981–5000, Oct. 2010.

Fangqing Wen (Member, IEEE) was born in China in 1988. He received the B.S. degree in electronic engineering from Hubei University of Automotive Technology, Shiyan, China, in 2011, and the postgraduation and Ph.D. degrees from the College of Electronics and Information Engineering, Nanjing University of Aeronautics and Astronautics, Nanjing, China, in 2013 and 2016, respectively.

From October 2015 to April 2016, he was a Visiting Scholar with the University of Delaware, Newark, DE, USA. Since 2016, he has been with the Electronic and Information School, Yangtze University, Jingzhou, China, where he is currently an Assistant Professor. His research interests include MIMO radar, array signal processing, and compressive sensing.

Dr. Wen is an Associate Editor of *Electronics Letters*. He is a Senior Member of the Chinese Institute of Electronics.

Juan Wang is currently pursuing the master's degree in communication and information engineering with the Nanjing University of Posts and Telecommunications, Nanjing, China.

Her research interest includes machine learning for wireless communications.

Junpeng Shi received the M.Sc. and Ph.D. degrees from Air Force Engineering University, Xi'an, China, in 2014 and 2018, respectively.

He is currently a Lecturer of information and communication engineering with the National University of Defense Technology, Hefei, China. His current research interest includes tensor signal processing with sparse MIMO radar.

Guan Gui (Senior Member, IEEE) received the Dr.Eng. degree in information and communication engineering from the University of Electronic Science and Technology of China, Chengdu, China, in 2012.

From 2009 to 2014, he was a Research Assistant and a Postdoctoral Research Fellow with the Wireless Signal Processing and Network Laboratory (Prof. Adachi Laboratory), Department of Communications Engineering, Graduate School of Engineering, Tohoku University, Sendai, Japan. From 2014 to 2015, he was an Assistant Professor with the Department of Electronics and Information System, Akita Prefectural University, Akita, Japan. Since 2015, he has been a Professor with Nanjing University of Posts and Telecommunications, Nanjing, China. He has published more than 200 international peer-reviewed journal/conference papers. He is currently engaged in the research of deep learning, compressive sensing, and advanced wireless techniques.

Prof. Gui received the Member and Global Activities Contributions Award from IEEE ComSoc and seven best paper awards, i.e., ICEICT 2019, ADHIP 2018, CSPS 2018, ICNC 2018, ICC 2017, ICC 2014, and VTC 2014-Spring. He was also selected as a Jiangsu Specially Appointed Professor in 2016, the Jiangsu High-Level Innovation and Entrepreneurial Talent in 2016, the Jiangsu Six Top Talent in 2018, and the Nanjing Youth Award in 2018. He was an Editor of *Security and Communication Networks* from 2012 to 2016. He has been an Editor of the IEEE TRANSACTIONS ON VEHICULAR TECHNOLOGY since 2017, IEEE ACCESS since 2018, the *KSII Transactions on Internet and Information Systems* since 2017, and the *Journal of Communications* since 2019, and the Editor-in-Chief of the *EAI Transactions on Artificial Intelligence* since 2018.